Regenerative Therapy 25 (2024) 194–202

Contents lists available at ScienceDirect

Regenerative Therapy

journal homepage: http://www.elsevier.com/locate/reth

Original Article

In vitro and functional investigation reveals the curative effect of thymoquinone from black cumin-loaded chitosan nanoparticles on streptozotocin induced paediatric diabetes

Qiuyan Xue, Yingrong Lin*

Department of Pediatrics, The First People's Hospital of Wenling, Wenling-317500, China

ARTICLE INFO

Article history:
Received 19 October 2023
Received in revised form
7 December 2023
Accepted 17 December 2023

Keywords:
Paediatric diabetes
Streptozotocin
Thymoquinone
Chitosan nanoparticle

ABSTRACT

Diabetic ketoacidosis (DKA) is regarded to be a communal complication of both type 1 and type 2 diabetes mellitus in children and adolescents. Successful therapy of DKA in children requires prompt diagnosis, strict monitoring of medical indicators, and prompt action. Thymoquinone (Tq) from black cumin loaded chitosan nanoparticles (ChNPs) intend to assess an effective agent to overcome this problem. XRD, FTIR, SEM, and TEM were used in the physicochemical analysis. Enzymatic activity of α-amylase and α-glucosidase was used in *in vitro* tests of anti-diabetic efficacy. Protecting insulin against enzyme breakdown is a crucial part of the insulin delivery mechanism. In the STZ-induced diabetes RIN-5F cell line, the anti-apoptotic capability of Tq-ChNPs was demonstrated through the NF-κB mediated apoptotic pathway. The combination of thymoquinone and chitosan NPs demonstrated that a wide variety of incredibly effective substances to elevate their curative effects, thus contributing to the growth of clinical and pharmaceutical fields.

1. Introduction

DKA is the most common diabetes-related cause of mortality in children [1,2]. DKA rates upon type 1 diabetes diagnosis have varied from 15 % to 83 % with most North American and European studies finding 40 % [3,4]. Depending on population socioeconomics and ethnicity, Asymptomatic urine screening detects most new instances of diabetes in Japanese children and adolescents [5], however 5 % of type 2 diabetes patients had DKA at diagnosis [6]. 25 % of children with Type 2 Diabetes Mellitus have DKA upon diagnosis [7]. This is most prevalent in African-American, least likely in Hispanic, and least probable in Canadian First Nation teens [8]. New-onset type 1 diabetes in young children is associated with DKA [9]. Infections, insulin omission, or insulin pump failure may cause DKA in children with diabetes. DKA is the leading cause of paediatric diabetes-related deaths, despite a 0.5 % fatality rate. Cerebral edoema causes 62%–87 % of DKA mortality. DKA is caused by insulin shortage and elevated levels of counterregulatory hormones such catecholamines, glucagon, cortisol, and growth hormone [10,11]. Absolute insulin insufficiency occurs in previously undiscovered type 1 diabetes mellitus (T1DM) and when patients on treatment intentionally or unintentionally skip insulin, particularly the long-acting component of a basal-bolus regimen [12]. Infants seldom have the “adult” triad of polyuria, polydipsia, and weight loss, making diabetes mellitus diagnosis difficult. This may partly explain the greater severity of first-presentation DKA in this age group [13]. Nano formulations' therapeutic properties provide anticipated results with these problems, helping to control the clinical severity. In order to investigate the effects of thymoquinone from black cumin coated with chitosan nanoparticles, this research was created. Herbal remedies have recently gained popularity as an adjunct to oral antidiabetic drugs as a result of the numerous studies that have shown their beneficial synergistic effects. Additionally, *Nigella sativa* (NS) is thought to be safer than oral antidiabetic medications [14]. The seeds of the black cumin plant, *Nigella sativa* L., a member of the Ranunculaceae family, are often used as culinary spices. The Unani, Ayurvedic, and Chinese systems of medicine have all employed *Nigella sativa*'s seeds, oils, and

* Corresponding author. No. 333, Chuanan South Road, Chengxi Street, Wenling, 317500, China
E-mail address: Yingrong.Lin134@hotmail.com (Y. Lin).
Peer review under responsibility of the Japanese Society for Regenerative Medicine.

https://doi.org/10.1016/j.reth.2023.12.012

extracts as medicinal agents for centuries. Thymoquinone (Tq), one of the key bioactive chemicals that was shown to have a protective effect against diabetes [15], is primarily responsible for the therapeutic actions of these plants. This study has looked at the use of herbal remedies to treat diabetes problems brought on by streptozotocin (STZ). The use of nanosized drug carriers can solve the problems of inadequate bioavailability and systemic side effects. It is possible that NPs can improve the absorption through the mouth and intravenous tissue retention of poorly soluble medications by adhering to the capillary walls. Experiments with higher doses to increase absorption were successful, although they were toxic to a number of vital organs [16]. In order to make accurate predictions about drug bioavailability, it is necessary to choose medicinal plants and their compounds that possess optimal hydrogen bonds, molecular weights, partition coefficients, log P-values, and rotatable bonds. Despite its low priority in cancer prevention, bioavailability of the relevant chemical at the target site is of the utmost importance. According to research by Maksymchuk et al. [17] black cumin (*Nigella sativa*) seed oil and the main chemical in it, thymoquinone, have shown anti-hyperglycemic efficacy in STZ-induced diabetes. The findings also revealed that the therapy may have protected against issues with organs connected to diabetes. It is also known that nanoparticles have a wide range of activities, and current research on nanoparticles for the treatment of infectious diseases and black cumin has shown anti-obesity and anti-diabetic outcomes through elevating phosphorylated Sirtuin 1 (SIRT1) levels in skeletal muscle and liver and activated protein kinase (AMPK) in the muscle [18]. When streptozotocin acts on B cells, it causes noticeable changes in the levels of insulin and glucose in the blood. The process by which pancreatic B cells absorb STZ involves the glucose transporter (GLUT2). One way to stop STZ from making people diabetic is to lower their GLUT2 expression. One possible explanation for STZ's toxicity is its strong alkylating capabilities. While STZ is responsible for DNA damage, the combined effects of nitric oxide (NO) and reactive oxygen species (ROS) may amplify these negative effects. Peroxynitrate, a very poisonous compound, can be formed when reactive oxygen species and NO react independently. Thus, STZ toxicity is significantly reduced by intracellular antioxidants or NO scavengers [19]. Due to its ability to keep -cells in good shape, black cumin has lately gained interest as an anti-diabetic drug. This plant possesses a novel medicinal potential due to the significant role of diabetes mellitus plays in global mortality rates. Uncontrolled diabetes can cause damage to multiple organ systems. Therefore, developing various drug delivery methods to enhance the oral bioavailability of hydrophobic phytochemicals is crucial. The capacity of cationic polymeric nanoparticles (NPs) to deliver lipophilic compounds on to the locations of their operations even as minimising off-target effects has drawn the attention of researchers. Chitin is partially deacetylated to produce the polymer known as chitosan (Cs). It is a kind of natural cationic polysaccharide that is risk-free, non-toxic, and non-antigenic. It has a long history of usage as a nanoparticle carrier [20]. Through electrostatic self-assembly, thymoquinone and chitosan may be used to create chitosan nanoparticles. The medicine is embedded in a lipid core of the nanoparticles, which have a coating of chitosan covering the core [21]. Patients are now able to choose from a wide variety of synthetic anti-diabetic medications, such as oral synthetic hypoglycemic treatments like sulfonylureas group, parenteral insulin therapy, and particular enzyme inhibitors like acarbose and miglitol. Despite their usefulness, these medications are prohibitively costly and are often linked to symptoms such as insulin resistance, bulimia nervosa, brain shrinkage, hepatotoxicity, stomach discomfort, and flatulence [22,23]. By improving peripheral glucose utilisation, lowering hepatic glucose output, and inhibiting gluconeogenesis, Tq improves glycemic status in diabetes [24]. People who have trouble digesting glucose may find relief with Tq since it lowers insulin resistance, glucose uptake, hepatic gluconeogenesis, blood sugar, cholesterol, triglycerides, and overall body mass index [25]. Like metformin, it improves glucose tolerance by mimicking the releases of insulin from pancreatic beta cells in response to glucose [26]. Therefore, the reason for this research was to define and describe nanoparticles of thymoquinone and chitosan were synthesised utilising a range of preparation methods. To improve Tq's therapeutic potential against juvenile diabetes, however, thymoquinone has not yet been formulated into thymoquinone-loaded chitosan nanoparticles (Tq-CsNPs). As a result, *In vitro* tests were performed on the produced NPs. Our primary goal was to demonstrate the efficacy of the nanosized product in addressing challenging cases of paediatric diabetes. Both α-amylase and α-glucosidase have been shown to have anti-diabetic effects. Tq-ChNPs' direct anti-diabetic action on RIN-5F cells and its positive effects were also investigated. Tq-ChNPs have an apoptotic effect in RIN-5F cell lines through modulation of Bcl-2 and Bax variants of NF-kB. The NPs' capacity to cure paediatric diabetes if too much thymoquinone or chitosan is present in them.

2. Methodology

2.1. Synthesis of thymoquinone loaded chitosan nanoparticles

Chitosan nanoparticles (Cs NPs) were created using an anionic gelation technique by Anand Raj et al. [27]. In brief, 50 mL of 1 % acetic acid solution and 500 mg of 85 % deacetylated chitosan were combined, and the mixture was agitated at 1000 rpm for 25 min until it was clear. The solution was sonicated to a pH of 5, and then 1 mg/mL of TPP was added and combined and this led to Cs NPs. The already-made Cs NPs were combined with 45 mg of Tq and 5 mL of DMSO to create Tq-Cs NPs. Before being collected by cooling spinning for 35 min at 14,000 rpm, rinsed under lyophilized conditions, using distilled water using a freeze dryer, the liquid was agitated for 2 h.

2.2. Characterization

Powdered X-ray diffraction (XRD) (X'PERT PROPAN analytical, PHILIPS, USA) was used to determine their degree of crystallinity. Debye Scherrer's formula, $D = 0.94/\cos\theta$, where k is the wavelength of the X-ray, b is the widest point along the ZnO line, and h is the angle of diffraction, was used to determine the size of the crystals in Tq-Ch NPs [28]. FTIR was used to pinpoint the functional groups between 4.5 and 0.5 μm. The FTIR data was acquired using a Bruker (Vertex 70 FTIR-FT Raman) spectrometer, gathered Tq, Tq-Cs NPs, Cs, and Cs NPs spectra. The spectra were averaged across three scans with a resolution of 1 cm^1. Using photon correlation spectroscopy or dynamic light scattering, the zeta potential, hydrodynamic size, polydispersity index value, and colloidal stability of dispersed CsNPs, Tq, and Tq-CsNPs were examined (DLS). Distilled water was utilised to keep the sample volume constant throughout analysis (1 mL). The zeta potential of stabilised Tq-Ch NPs was evaluated using a 90 plus particle size analyzer (Brookhaven Instruments Corporation, Holtsville, NY, USA [29]. The Hitachi S-4500 was used as a SEM to look at the Tq-Ch NPs. The synthesised and stabilised formulations were created on a copper grid coated with carbon by simply dropping a very little bit of the sample on the grid, wiping off any excess solution using blotting paper, and letting the films dry for 5 min under a mercury lamp. Synthesised Tq-Cs NPs were scanned at 300 kV by means of a high-resolution transmission electron microscope (TEM, JEM 1400, software DM-3, Japan) to determine their surface shape and particle size.

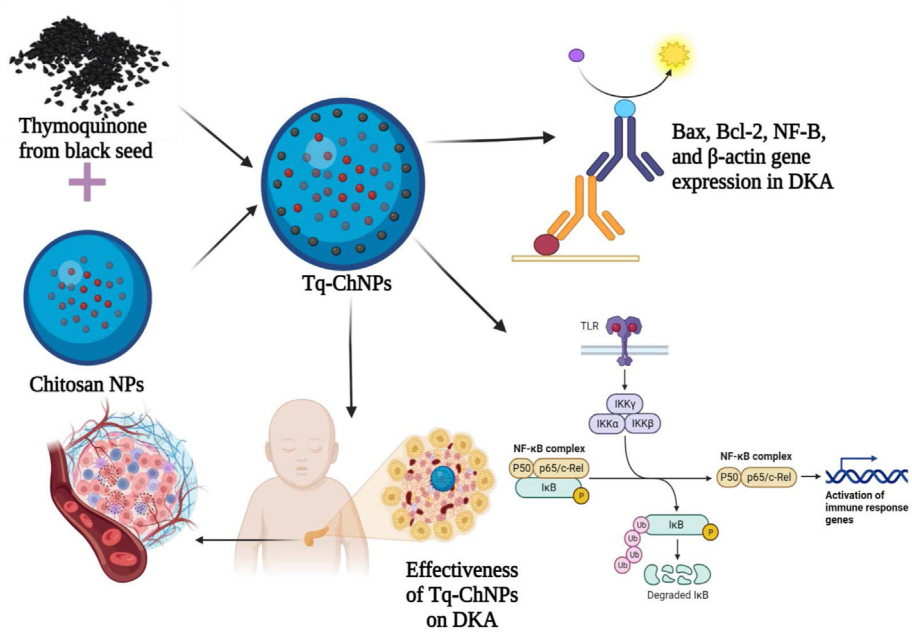

Fig. 1. Schematic representation of Tq-ChNPs and its potential on DKA.

2.3. *In vitro antidiabetic assays*

2.3.1. *α-amylase activity*

A test tube was filled with a mixture that was homogeneously mixed with 250 ml of Tq-Ch NPs at various concentrations (20, 40, 60, 80, and 100 μg/mL), 250 ml of starch 2.0 % (w/v), and 250 ml of a solution containing 1 U ml^{-1} α-amylase. The enzymatic reaction was stopped by adding 500 μl of a colourant (dinitrosalicylic acid, DNS) after 3 min of incubation at 20 °C. After keeping the mixture in boiling water, 250 μl of α-amylase was added right away. For 15 min, the mixture was heated. After that, it was cooled and mixed with 5 ml of distilled water. The control group followed the same protocol as the test groups, except they used distilled water instead of extract. The % inhibition was determined by taking the absorbance of each test tube content at 540 nm [30].

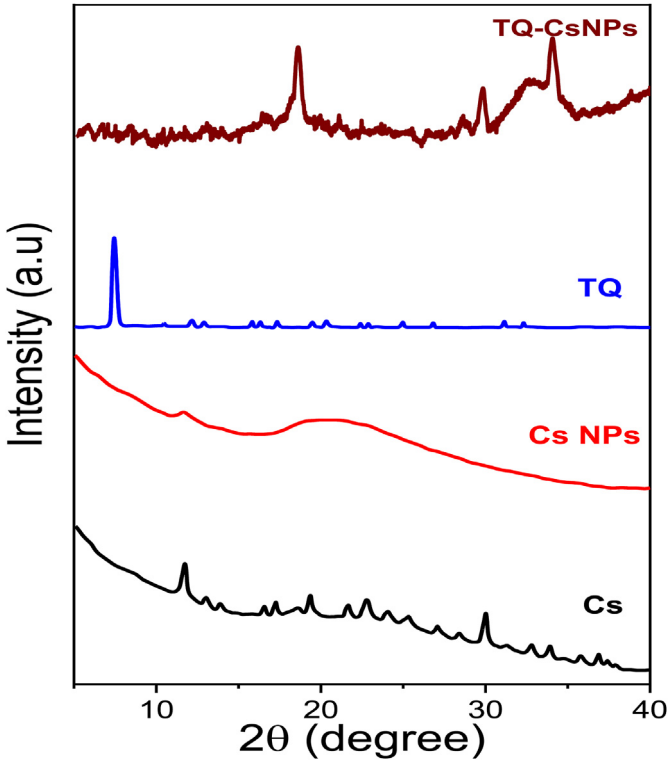

Fig. 2. XRD analysis of Cs, Cs NPs, Tq and Tq-ChNPs.

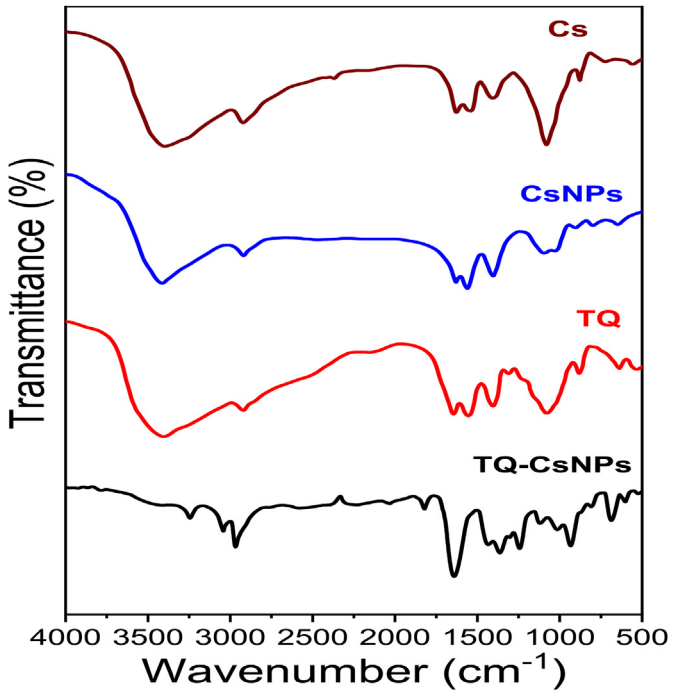

Fig. 3. FTIR analysis of Tq-ChNPs, Tq, Cs NPs and Cs peak patterns and positions varied significantly.

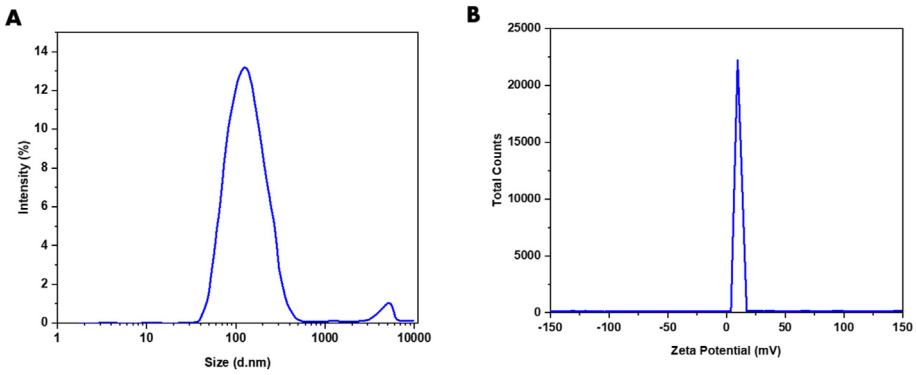

Fig. 4. A) Hydrodynamic size and distribution of Tq-ChNPs B) Zeta potential of Tq-ChNPs.

2.3.2. α-glucosidase activity

Mixtures of 0.1 M of phosphate buffer solution, 50 μl of different amounts of Tq-Ch NP (20, 40, 60, 80, and 100 μg/ml), and 5 mM 4-nitrophenyl-D glycol pyranoside (PNPG) substrate were kept at 37 °C for 5 min. Then, starting with a total of Each well was supplemented with 100 μl of an α-glucosidase solution containing 0.15 U ml^{-1}. After 15 min of mixing, 100 μl of 200 mM sodium carbonate was added to stop the process. With the help of a microplate reader, 405 nm was found to be the absorption. After each test was done three times, the results were added up [31].

2.3.3. Maintenance of cell culture

RIN-5F cell lines were placed in a controlled environment with a relative humidity of 70 % and 5 % carbon dioxide (CO_2) in Roswell Park Memorial Institute (RPMI) medium that was enhanced with 10 % foetal bovine serum, 100 μg/ml of streptozotocin, and 100 U/ml of penicillin.

2.3.4. Cell culture therapy

After growing RIN-5F cells to 80 % added in RPMI-1640 with 10 % foetal calf serum, the cells were treated with Tq-Ch NP solution in 10 mM citrate buffer (pH 4.5). There were five distinct sets of cells used in this study. Normal RIN-5F cells (Group 1), RIN-5F cells uncovered to streptozotocin (10 mM) for 24 h (Group 2), RIN-5F cells treated with Tq-Ch NP (15, 30, or 60 μg/ml) for 24 h (Groups 3, 4, and 5). The cells were collected after treatment and rinsed in a medium buffer containing a little amount of phosphate-buffered saline (PBS). Mitochondrial content was extracted through centrifugation-based cellular fractionation.

2.3.5. MTT test

The 96 well plates were used for the cell viability experiment based on the mitochondrial reductase enzyme. Approximately 5×10^3 streptozotocin-treated cells were employed per well. After 24 h incubation, the cells were treated with 10 min with Tq-Ch NP at several doses. Following incubation, 100 μl (1 mg/ml) of MTT, a tetrazolium dye solution, was added to the cells for 4 h without refrigeration, and then the medium containing MTT was removed and swapped with 100 μl of dimethyl sulfoxide. The ELISA reader was used to measure the intensity of the purple crystal formed when MTT was converted into formazan. Absorbance was measured at 570 nm, and results were analysed in comparison to cells used as controls.

2.3.6. Staining for apoptosis

DAPI (1 mg/mL) and 2,7-dichlorodihydrofluorescein diacetate (DCF-DA) in PBS were used to stain nuclei in order to observe morphological alterations brought on by apoptotic stimuli. Briefly stated, 6 well plates of RIN5F (5×10^5 cells) were cultivated before being treated to STZ and Tq-Ch NP for 24 h. After two PBS buffer washes, the cells were stained. The cells were analysed using fluorescent microscopy with a 377–355 nm filter.

2.3.7. Flow cytometric evaluation of apoptosis

Streptozotocin (10 mM) was added to 6-well plates containing RIN-5F cell lines, and the plates were incubated for 24 h to detect apoptosis using flow cytometry. Tq-Ch NP was then given to the cells for 24 h. The cells were stained with annexin-V/PI after a 24-h exposure to Tq-Ch NP at a concentration of 60 μg/ml 100 μl of cell suspension were treated with 5 μL of propidium iodide (PI) and 5 μl of Annexin V conjugated to fluorescein is incubated in a dark room at 25° Celsius for 15 min. Flow cytometry was used to detect apoptosis after 400 μl of binding buffer was added to the suspension (Becton Dickinson FACSc an, CA, USA).

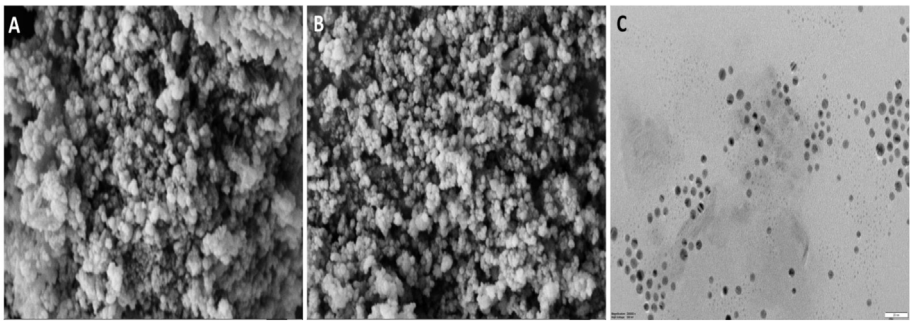

Fig. 5. A), SEM images of Cs NPs and B) Tq-CsNPs; C) TEM image of Tq-CsNPs.

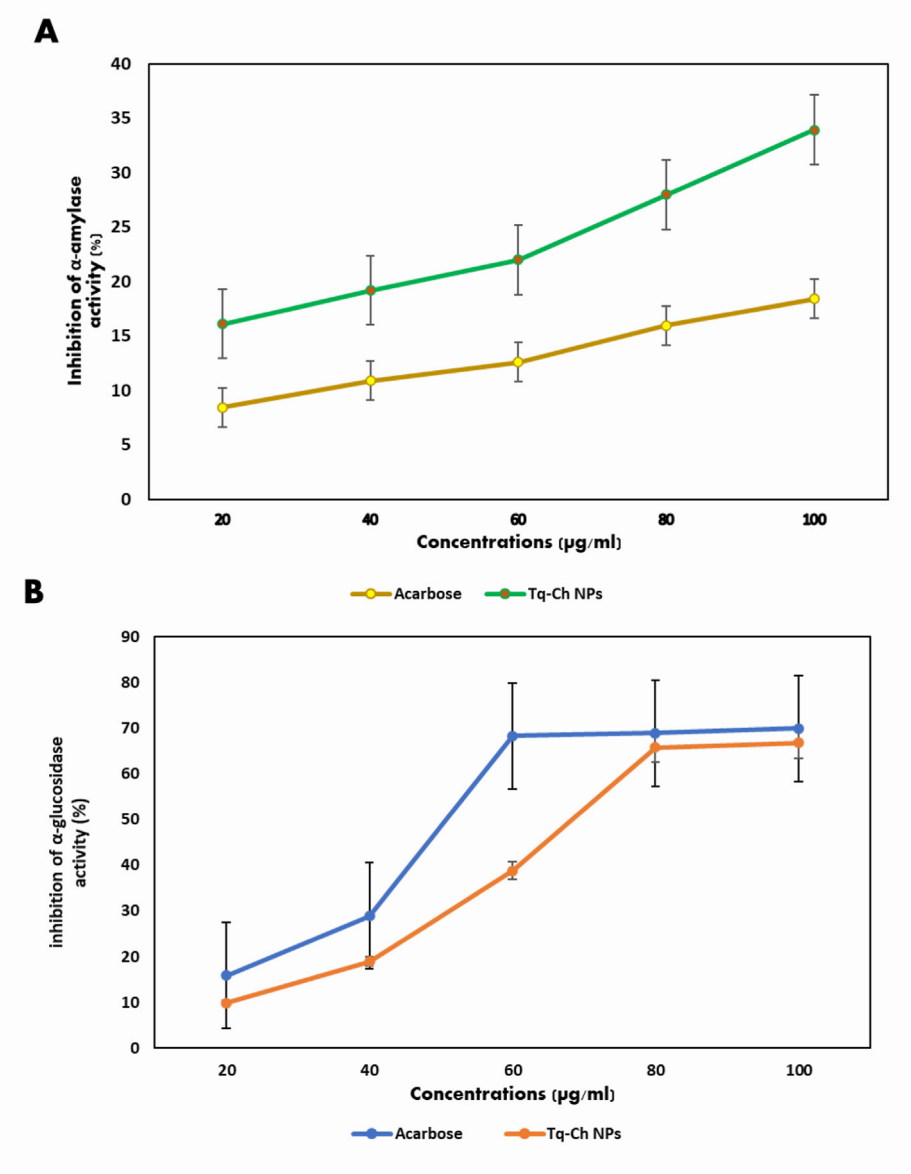

Fig. 6. In vitro antidiabetic activity of Tq-CsNPs with A) α-amylase activity and B) α-glucosidase activity. Results were plotted with mean ± standard deviation of three replications and statistical significance at $P \leq 0.05$ using ANOVA followed by Tukey's HSD test.

2.3.8. The western blotting method

RIPA (Ingredients (1X lysis buffer, 1X protease inhibitor cocktail, PMSM-1Mm, and water) were used to lyse the cells after a quick wash in DPBS. The buffer was centrifuged and placed in the freezer to speed up the dissolution of the clumps. Using a syringe, the lysate was extracted. After incubating on frozen ground for 30 min, the lysate was spun at high speed in a centrifuge. The Folins Lowry method, as outlined by Markwell et al. [32], was used to determine the protein content. A reference point for comparison was BSA. Warming the SDS sample buffer dissolved the samples. Using an attempting to resolve gel concentration ranging from 6 to 10%, we separated the proteins using SDS-PAGE. For the samples, a mixture of 20 µl and approximately 30 µg of protein was prepared. The proteins were forwarded to a PVDF membrane after the gel was run. The membrane had previously been submerged in methanol for a duration of 2 min. In the transfer cassette, the gel and membrane were positioned such that the membrane faced the cathode. Every hour of the night, the membrane-gel sandwich cassette was submerged in 20 V transfer buffer. Upon transfer, the membrane was rinsed three times with 25 ml of TBS for 5 min. Subsequently, it was incubated for 1 h in 25 ml of blocking solution, which consisted of non-fat dry milk, Tween 20, and TBS. Primary antibodies against Bax, Bcl-2, NF-B, and β-actin were next applied to the blotted

Table 1
The effects of Tq-ChNPs on cell viability in Streptozotocin induced apoptosis pancreatic β-cells. In this table the values are given in mean ± SD.

Cell lines (µg/ml)	% of cell viability
Normal RIN-5F cells	100.0 ± 6.9^{a}
Streptozotocin	43.02 ± 3.4^{b}
Tq-ChNPs (20 µg/ml)	51.02 ± 2.9^{b}
Tq-ChNPs (60 µg/ml)	62.09 ± 3.5^{c}
Tq-ChNPs (100 µg/ml)	70.04 ± 4.8^{d}

Different alphabets indicates significant among groups ($p < 0.05$).

membrane following three washes in TBST (Tris-buffered saline with tween). After that, the membrane was incubated in blocking solution with a secondary antibody that was conjugated to horseradish peroxidase for 1 h at room temperature. After a 5-min wash in TBST, we used enhanced chemiluminescence to identify the target protein (ECL).

2.3.9. Statistical analysis

All of the trials were conducted on three separate occasions. We ran the statistical models on the data using GraphPad Prism 8.0, which is developed by GraphPad Software and is located in California, USA. To compare means, the data were subjected to a one-way ANOVA test. For comparisons that involved more than one variable, an appropriate post hoc test had also been run. A p-value of less than 0.05 was considered to indicate statistical significance.

3. Results and discussion

3.1. Characterization

The main objective of this study was to prove the effectiveness of the nano-sized product in treating difficult instances of paediatric diabetes. The anti-diabetic effects of both α-amylase and α-glucosidase have been demonstrated. Fig. 1 shows the detailed scheme representation of Tq-ChNPs and its potential on DKA. X-ray diffraction research verified that Tq-ChNPs exist in a crystalline phase. Bragg's reflection peaks of hexagonal phase were seen in the XRD patterns of Cs, CsNPs, Tq, and Tq-ChNPs (Fig. 2). These peaks were located at 2 = 10.2°, 10.5°, 0.5°, and 35.7°. As the Cs chains dissolved, they left behind a single floppy peak in an otherwise opaque network topology. A loss of periodicity and crystallinity is reflected in a decrease in crystallite size, which was indicated by the appearance of a wide peak [33]. The nanoscale crystal structure of Tq was determined by high-resolution X-ray powder diffraction, providing insight into Tq's chemical role. A 10-0.40313-point peak at 8.4997 with a 100 % relative intensity were seen in the XRD spectrum of Tq collected for this investigation, that agrees with the previous Rietveld refinement XRD of Tq on the base scale [34]. It was challenging to identify faint signals due to Bragg's peaks that overlapped. Taking into account the conventional Tq solid's infrared spectrum. The Tq-ChNPs surface functional groups were identified using FTIR (Fig. 3). The sharp, strong, and weak peaks in the spectra of Tq confirmed that the characteristic peak identified at 1702 cm^1 was due to the presence of Tq, together with the essential functional groups C—H, —CH2, —CH3, C—O, and C—C. Mohammed et al. [35] observed that the peaks in the spectra were consistent with those previously reported in the literature. Hydrogen bonding might be responsible for the size difference between Cs and CsNPs. Maximum frequencies for aliphatic C—H stretching are reported by Nivethaa et al. [36] to be 2900 cm^{-1}, for N—H bending to be 1662 cm^{-1}, for primary alcoholic C—O stretching to be 1414 cm^{-1}, and for hydroxyl group C3 stretching to be 1098 cm^{-1}. Tq-CsNPs size distribution as a function of reported intensity. The intensity distribution's size was compared to the measured cumulant fit. The Tq-CsNPs exhibit a mean hydrodynamic diameter (Z) of 92.25 nm, as determined by dynamic light scattering (DLS) research. The determination of the zeta potential value of Tq-ChNPs provided insights into their surface charge and stability characteristics. The electrical conductivity of the substance was measured to be 0.321 mS per centimeter (mS/cm), while its zeta potential was determined to be 15.36 mV (mV) as shown in Fig. 4. Nanoparticle surface charges and thermodynamic stability were investigated using the zeta potential. According to the standard norm, carboxy methyl hexanoyl Cs has a high zeta potentiality

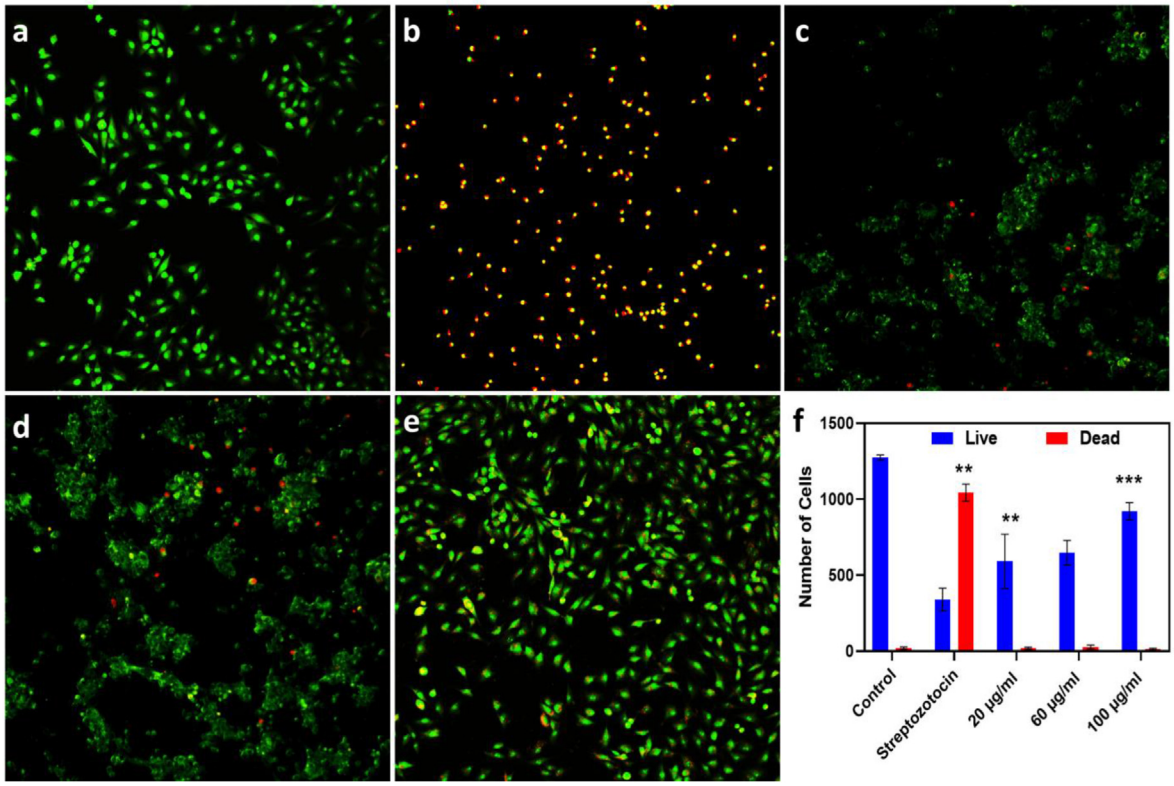

Fig. 7. Live and dead cell assay of RIN-5Fcells treated with PBS Control at 10× magnification, 100 nm (a), Streptozotocin (b), treated with Tq-CsNPs at 20 μg/ml (c), Tq-CsNPs at 60 μg/ml (d), Tq-CsNPs at 100 μg/ml (e).

of +47.2 mV, which is consistent with the high ionic conductivity and sufficient nutrient carrier stability observed in CsNPs; a surface charge of +30 mV or less, or −30 mV or less, can prevent particle aggregation [37]. According to the CsNPs, the surface's texture was not consistent but rather rough and uneven, with obvious straps and shrinkage. The formation of Tq-CsNPs is achieved by the fusion of two water-based phases, one comprising polymer Cs and another of poly-anion. However, the SEM image and the manufacturing process don't appear to line up. The spherical form and average particle size of the synthesised CsNPs (Fig. 5. A) and (Fig. 5. B) Tq-CsNPs, which is around 50 nm, are clearly visible. In TEM images of Tq-CsNPs showed (Fig. 5. C) spherical shape, whereas high resolution transmission electron microscopy (TEM) of Tq-CsNPs with a narrow field of view showed that the resulting Tq-CsNPs were shaped like rhombohedra [38].

3.2. *In vitro antidiabetic assays*

3.2.1. *α-amylase activity*

In the current investigation, demonstrated a considerable, concentration-dependent suppression of α-amylase enzyme activity. Tq-CsNPs at doses of 20, 40, 60, 80, and 100 μg/ml inhibited the activity of the α-amylase enzyme by 7.67, 8.3, 9.4, 12.01 and 15.49 %, respectively. At the same doses, the reference standard acarbose inhibited α-amylase activity by 8.45, 10.9, 12.6, 15.98, and 18.43 % (Fig. 6 A). The hydrolysis of α-1,4-glycosidic bonds in starch, glycogen, and other oligosaccharides is catalysed by alpha amylase. Inhibiting their function in the human digestive system is thought to be a useful method for managing diabetes. Additionally, these outcomes could result in a reduction in the absorption of monosaccharides. α-amylase inhibitors that are efficient and safe have so long been searched after. Starch decreased alpha-amylase's catalytic activity *in vitro*.

3.2.2. *α-glucosidase activity*

Tq-CsNPs values were discovered to have their glucosidase activity, which inhibits α-glucosidase. When α-glucosidase inhibition took place, it resulted in glycemic control by the addition of these natural Tq-CsNPs molecules in *in vitro* tests (Fig. 6 B). According to the *in vitro* data, the cereal Tq-CsNPs possesses antidiabetic qualities. Tq-CsNPs at doses of 20, 40, 60, 80, and 100 μg/ml inhibited the activity of the α-amylase enzyme by 9.87, 18.97, 38.8, 65.8 and 66.8 % respectively. At the same doses, the reference standard acarbose inhibited α-amylase activity by 15.87, 28.98, 68.3, 68, and 69.98. Similar to this, α-glucosidase activity has a mild inhibitory effect on glucose absorption. Consequently, the results indicate that produced from barley G functions as a potential antidiabetic drug [39].

3.2.3. *MTT assay*

With 45 % at 10 mM, cell death was achieved. RIN-5F cells treated with Tq-Ch NP, however, displayed improved cell viability in response to the cytotoxicity caused by STZ. In order to assess the RIN-

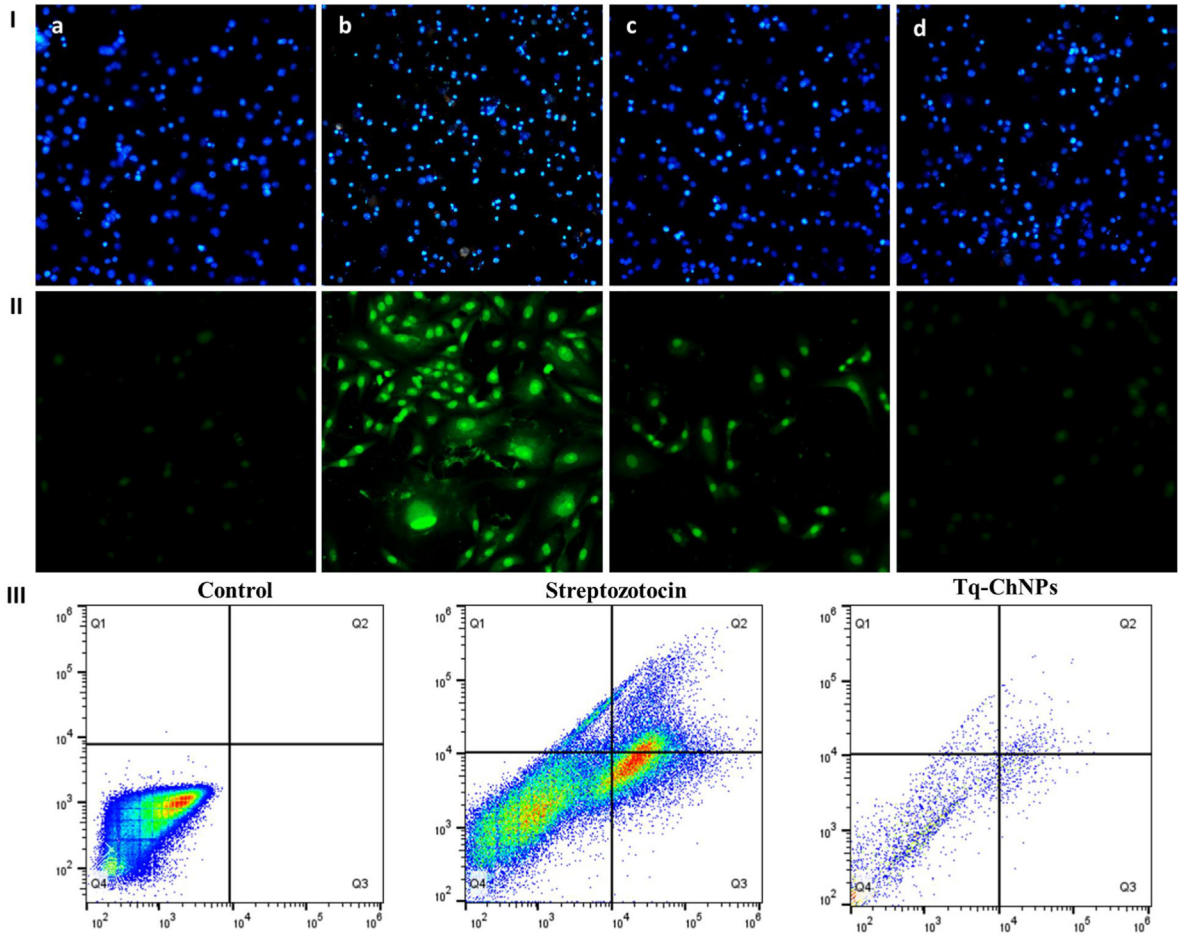

Fig. 8. Effects of Tq-ChNPs on DEHP induced apoptosis features in RIN-5F cells at 10× magnification, 100 nm, I) DAPI stain; Control (a), Streptozotocin (b), treated with Tq-CsNPs at 60 μg/ml (c), Tq-CsNPs at 100 μg/ml (d). II) ROS. (III) The cell death percentage stained with annexin-V/PI with flow cytometer.

5F cells' viability, MTT test was performed (Table 1). Different STZ concentration ranges were used to treat the cells. It was discovered that STZ 10 mM for 24 h drastically reduced cell viability performed with Control, treated with streptozotocin, treated with Tq-Ch NP at three different concentrations 20, 60, 100 μg/ml showed in Fig. 7a–f respectively. Additionally, this is similar to the result, it has been shown that pancreatic β-cells necrosed in response to large doses of STZ, but low doses of STZ produced cell death through apoptosis [40]. Similarly, after being treated with STZ, cell viability, as measured by the MTT assay, was shown to drop by around 40 %. The cellular viability of streptozotocin-treated cells was significantly enhanced by pre-treatment with N-acetylcysteine (NAC) [41]. After being treated with the extract for 24 h, cells that had been pre-treated with STZ showed increased vitality when administered with concentrations of 10 and 100 μg/mL of the extract, respectively. The p-values for these treatments were 0.1667 and 0.0564, suggesting a tendency towards significance. There was no discernible improvement in cell viability after 48 or 72 h of therapy [42]. RIN-5F cells, a cell line generated from rat islet tumors, to analyze insulin secretion in order to assess the effect of nymphayol on this biological process. There was a dose-dependent effect of the molecule Nymphayol on insulin secretion. Significant effects were observed in low glucose and high glucose conditions at values of 10 and 40 μM, respectively. Thus, it can be inferred that nymphayol's effects on insulin secretion are not due to cytotoxicity [43].

3.2.4. Apoptosis evaluation using flow cytometry

Increased ROS production and the oxidative stress it created directly triggered a number of metabolic abnormalities and apoptosis under these conditions [44]. The effects of ROS-derived oxidative stress include lipid peroxidation and lipotoxicity, which damage proteins and cause the pancreatic beta-cells to continually degrade, particularly in hyperglycemic circumstances [45]. Using staining techniques an examination of the cellular and nuclear morphology has been carried out. The findings of the DAPI staining, which was used to see the DNA damage, are shown in Fig. 8aI & II. STZ-treated RIN-5F cells for 24 hoursexhibited a number of morphological changes in comparison to untreated cells, the most notable of which were aberrant nuclei, characterised by shattered nuclei and chromatin. Cell and nuclear damage were also reduced in RIN-5F cells following STZ treatment. As can be shown in Fig. 8b, after being treated with 10 mM STZ, RIN-5F pancreatic β-cells produced much more intracellular reactive oxygen species (ROS) than control RIN-5F cells. The amount of ROS in the cells was nonetheless decreased by Tq-ChNPs therapy as shown in Fig. 8c and d, different dosage of Tq-ChNPs at 60 and 100 μg/ml. When STZ containing were applied Tq-ChNPs to RIN-5F cells, the amount of apoptosis was calculated using a FACS test. The proportion of cells experiencing early/late apoptosis increased significantly when 10 mM STZ was used to trigger apoptosis for 24 h (Fig. 8. III), Flow cytometry analysis compared to groups of normal cell lines. After 24 h of treatment with Tq-ChNPs, programmed cell death in cells exposed to STZwas significantly reduced, suggesting that these particles might be used to prevent the loss of pancreatic beta cells. Similarly, pancreatic β-cell survival requires mitogen-activated protein kinase (MAPK) and numerous other intracellular and extracellular routes, phosphatidylinositol 3-kinase (PI3K), and nuclear factor (NF)—B [46]. By coordinating with Bax, Bak, Bcl-xS, and Bcl-xL, Bcl-2 regulates both apoptosis and anti apoptosis. The Bcl-2 family regulates apoptosis, and this is combined with a well-known death pathway in the apoptotic signal [47].

3.2.5. Western blot analysis

Therefore, as a result of our research, the reduced amount elevated Bcl-2 protein levels and Bax (Fig. 9A) shows that the cell

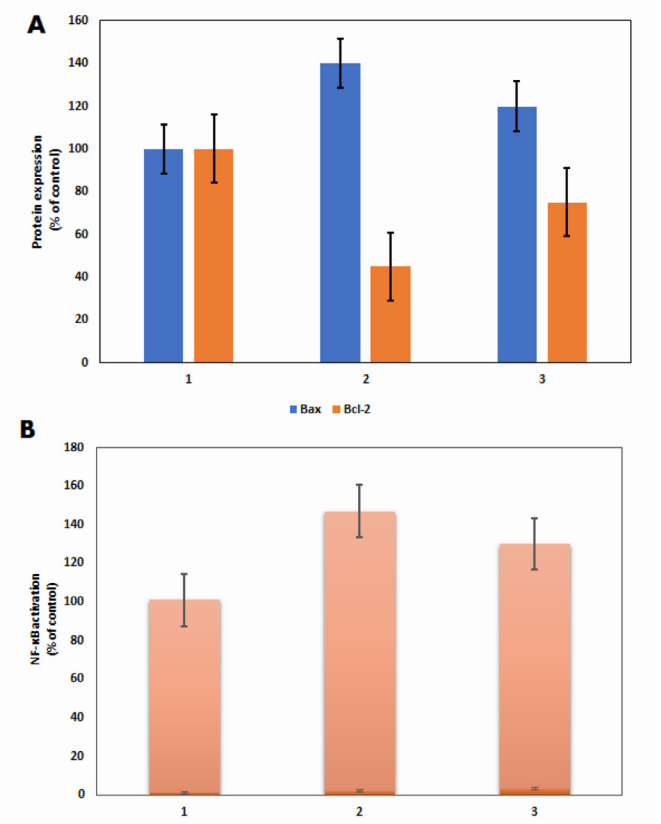

Fig. 9. Effect of Tq-ChNPs NF-kB activation and Protein expression of Bcl-2 and Baz in RIN-5F cell lines. Values includes means ± SD (n = 3) of all three individuals. (1. RIN-5F cells; 2. Streptozotocin, 3. Tq-ChNPs).

survival was stimulated via the NF—B pathway (Fig. 9B). Tq-Ch NP may have triggered this pathway in RIN-5F diabetic cells caused by STZ. It has been shown that a high level of anti-apoptotic protein production may protect pancreatic β-cells against the effects of STZ treatment. The results are comparable to the findings that were published by Varastea et al. [44], who said that the flavone compound cirsimaritin has the ability to protect INS-1 pancreatic β-cells from the considerable apoptosis that is generated by STZ.

4. Conclusions

Possible mechanisms and method of action in paediatric diabetes are provided by the current investigation. Tq-ChNPs have been shown to reverse streptozotocin-induced diabetes in children when tested for their anti-diabetic action *in vitro*. α-amylase and α-glucosidase enzymatic tests are examples of the antidiabetic activities. In addition, Tq-ChNPs were studied for their direct anti-diabetic impact on RIN-5F cells. Tq-ChNPs have an apoptotic effect in RIN-5F cell lines through modulation of Bcl-2 and Bax variants of NF-kB. These results provide compelling evidence that Tq-ChNPs may serve as the effective therapeutic agent for diabetes and other biomedical conditions. Therefore, Tq-ChNPs may be utilised without risk to cure diabetes in children. To determine its therapeutic effectiveness on persons with diabetes, a well-defined and suitably powered randomised controlled clinical study is urgently needed.

Declaration of competing interest

The authors have no competing financial interests to declare.

Acknowledgement

This study was supported by Scientific Research Project of Wenling Science and Technology Bureau, No. 2019S0180058; and Provincial Health Science and Technology Plan Project, No. 2021KY404.

References

[1] Edge J, Ford-Adams M, Dunger D. Causes of death in children with insulin-dependent diabetes. Arch Dis Childhood 1999;81:318–23.
[2] Scibilia J, Finegold D, Dorman J, Becker D, Drash A. Why do children with diabetes die? Eur J Endocrinol 1986;113:326–33.
[3] Levy-Marchal C, Patterson C, Green A. Geographical variation of presentation at diagnosis of type 1 diabetes in children: the EURODIAB study. Diabetologia 2001;44:75–80.
[4] Mallare J, Cordice C, Ryan B, et al. Identifying risk factors for the development of diabetic ketoacidosis in new onset type 1 diabetes mellitus. Clin Pediatr 2003;42:591–7.
[5] Yokota Y, Kikuchi N, Matsuura N. Screening for diabetes by urine glucose testing at school in Japan. Pediatr Diabetes 2004;5:212–8.
[6] Sugihara S, Sasaki N, Kohno H, Amemiya S, Tanaka T, Matsuura N, et al. Survey of current medical treatments for childhood-onset type 2 diabetes mellitus in Japan. Clin Pediatr Endocrinol 2005;14:65–75.
[7] Wolfsdorf J, Craig ME, Daneman D, Dunger D, Edge J, Lee W, Rosenbloom A, Sperling M, Hanas R. Diabetic ketoacidosis in children and adolescents with diabetes. Pediatr Diabetes 2009;10:118–33.
[8] Zdravkovic V, Daneman D, Hamilton J. Presentation and course of type 2 diabetes in youth in a large multi-ethnic city. Diabet Med 2004;21:1144–8.
[9] Blanc N, Lucidarme N, Tubiana-Rufi N. Factors associated with childhood diabetes manifesting as ketoacidosis and its severity. Archieves in Pediatrics 2003;10:320–5.
[10] Foster DW, Mcgarry JD. The metabolic derangements and treatment of diabetic ketoacidosis. N Engl J Med 1983;309:159–69.
[11] Kitabchi AE, Umpierrez GE, Murphy MB, Kreisberg RA. Hyperglycemic crises in adult patients with diabetes: a consensus statement from the American Diabetes Association. Diabetes Care 2006;29:2739–48.
[12] Hanas R, Lindgren F, Lindblad B. A 2-yr national population study of pediatric ketoacidosis in Sweden: predisposing conditions and insulin pump use. Pediatr Diabetes 2009;10:33–7.
[13] Wolfsdorf J, Glaser N, Sperling MA. Diabetic ketoacidosis in infants, children and adolescents. Diabetes Care 2006;29:1150–9.
[14] Pan SY, Zhou SF, Gao SH, Yu ZL, Zhang SF, Tang MK, Sun JN, Ma DL, Han YF, Fong WF, et al. New perspectives on how to discover drugs from herbal medicines: CAM's outstanding contribution to modern therapeutics. Evidence based complement. Alternat Med 2013;2013:25.
[15] Khader M, Eckl PM. Thymoquinone: an emerging natural drug with a wide range of medical applications. Iranian J Basic Med Sci 2014;17:950–7.
[16] Aqil F, Munagala R, Jeyabalan J, Vadhanam MV. Bioavailability of phytochemicals and its enhancement by drug delivery systems. Cancer Lett 2013 Jun 28;334(1):133–41. https://doi.org/10.1016/j.canlet.2013.02.032. Epub 2013 Feb 19. PMID: 23435377; PMCID: PMC3815990.
[17] Maksymchuk O, Shysh A, Rosohatska I, Chashchyn M. Quercetin prevents type 1 diabetic liver damage through inhibition of CYP2E1. Pharmacol Rep 2017;69:1386–92.
[18] Karandrea S, Yin H, Liang X, Slitt AL, Heart EA. Thymoquinone ameliorates diabetic phenotype in diet-induced obesity mice via activation of SIRT-1-dependent pathways. PLoS One 2017;12:0185374.
[19] Szkudelski T. The mechanism of alloxan and streptozotocin action in B cells of the rat pancreas. Physiol Res 2001 Jan 1;50(6):537–46.
[20] Jin L, Hua Y, Puligundla P, Gao X, Zhou Y, Wan X. Applications of chitosan nanoparticles to enhance absorption and bioavailability of tea polyphenols: a review. Food Hydrocolloids 2017;69:286–92.
[21] Ning S, Wang C, Zhao L, Yang J, Shi X, Zheng Y. Lecithin/chitosan nanoparticle drug carrier improves anti-tumor efficacy of Monascus pigment rubropunctatin. Int J Biol Macromol 2023;242:125058.
[22] Piedrola G, Novo E, Escobar F, Garcia-Robles R. White blood cell count and insulin resistance in patients with coronary artery disease. Annals of clinical Endocrinol 2001;62:7–10.
[23] Yaryura-Tobias JA, Pinto A, Neziroglu F. Anorexia nervosa, diabetes mellitus, brain atrophy, and fatty liver. Int J Eat Disord 2001;30:350–3.
[24] Darakhshan S, Bidmeshki Pour A, Hosseinzadeh Colagar A, Sisakhtnezhad S. Thymoquinone and its therapeutic potentials. Pharmacol Res 2015:95–6.
[25] Chen L, Li B, Chen B, Shao Y, Luo Q, Shi X, Chen Y. Thymoquinone alleviates the experimental diabetic peripheral neuropathy by modulation of inflammation. Sci Rep 2016 Aug 22;6(1):31656.
[26] Faisal Lutfi M, Abdel-Moneim AM, Alsharidah AS, Mobark MA, Abdellatif AA, Saleem IY, Al Rugaie O, Mohany KM, Alsharidah M. Thymoquinone lowers blood glucose and reduces oxidative stress in a rat model of diabetes. Molecules 2021 Apr 17;26(8):2348.
[27] Anand Raj L, Jonisha R, Revathi B, Jayalakshmy E. Preparation and characterization of BSA and chitosan nanoparticles for sustainable delivery system for quercetin. J Applied Pharmacol Sci 2015;5:1–5.
[28] Hajizadeh Z, Taheri-Ledari R, Asl FR. 3- Identification and analytical methods. In: Maleki A, editor. Heterogeneous micro and nanoscale composites for the catalysis of organic reactions. Elsevier; 2022. p. 33–51. Micro and nano technologies.
[29] Alam S, Khan ZI, Mustafa G, Kumar M, Islam F, Bhatnagar A, Ahmad FJ. Development and evaluation of thymoquinone-encapsulated chitosan nanoparticles for nose-to-brain targeting: a pharmacoscintigraphic study. Int J Nanomed 2012;7:5705–18.
[30] Elya B, Handayani R, Sauriasari R, Hasyyati US, Permana IT, Permatasari YI. Antidiabetic activity and phytochemical screening of extracts from Indonesian plants by inhibition of alpha amylase, alpha glucosidase and dipeptidyl peptidase IV. Pakistan J Biol Sci 2015;18:279–84.
[31] Dewi RT, Iskandar YM, Hanaf M, Kardono LBS, Angelina M, Dewijanti ID, Banjarnahor SDS. α-Glucosidase inhibitor compounds from Aspergillus terreus RCC1 and their antioxidant activity. Pakistan J Biol Sci 2007;10:3131–5.
[32] Markwell MA, Haas SM, Bieber LL, Tolbert N. A modification of the lowry procedure to simplify protein determination in membrane and lipoprotein samples. Anal Biochem 1978;87:206–10.
[33] Ferreira Tomaz A, Sobral de Carvalho SM, Cardoso Barbosa R, Gutierrez Sabino. Ionically crosslinked chitosan membranes used as drug carriers for cancer therapy application. Materials 2018;11.
[34] Pagola S, Benavente A, Raschi A, Romano E, Molina MA, Stephens PW. Crystal structure determination of thymoquinone by high-resolution X-ray powder diffraction. AAPS Pharmacol Sci Technol 2004;5:28.
[35] Mohammed SJ, Amin HHH, Aziz SB, Sha AM, Hassan S, Abdul, Aziz JM, Rahman HS. Structural characterization, antimicrobial activity, and in vitro cytotoxicity effect of black seed oil. Evidance Based Complement. Alternative Med 2019;2019:6515671.
[36] Nivethaa AK, Baskar S, Martin CA, Ramana RJ, Stephen A, Narayanan V, Lakshmi BS, Frank-Kamenetskaya OV, Radhakrishnan S, Narayana KS. A competent bidrug loaded water soluble chitosan derivative for the effective inhibition of breast cancer. Sci Rep 2020;10:3991.
[37] Larsson M, Borde A, Mattisson E, Liu D, Larsson. A Evaluation of carboxymethyl-hexanoyl chitosan as a protein nanocarrier. Nanomater Nanotechnol 2013;1:3–7.
[38] Hosni A, Abdel-Moneim A, Hussien M, Zanaty MI, Eldin ZE, El-Shahawy AA. Therapeutic significance of thymoquinone-loaded chitosan nanoparticles on streptozotocin/nicotinamide-induced diabetic rats: in vitro and in vivo functional analysis. Int J Biol Macromol 2022;221:1415–27.
[39] Mebrek S, Djeghim H, Mehdi Y, Meghezzi A, Sirajudheen A, Benali M. Antioxidant, anti-cholinesterase, anti-α-glucosidase, and prebiotic properties of β glucan extracted from Algerian barley. Phytomedicine 2018;10:58–67.
[40] Vijayakumar S, Vinayagam R, Anand MAV, Venkatachalam K, Saravanakumar K, Wang MH, Gothandam KM, David E. Green synthesis of gold nanoparticle using Eclipta alba and its antidiabetic activities through regulation of Bcl-2 expression in pancreatic cell line. J Drug Deliv Sci Technol 2020;58:101786.
[41] Lee SH, Kang SM, Ko SC, Kang MC, Jeon YJ. Octaphlorethol a, a novel phenolic compound isolated from Ishigefoliacea, protects against streptozotocin induced pancreatic β-cell damage by reducing oxidative stress and apoptosis. Food Chem Toxicol 2013;59:643–9.
[42] Coskun O, Kanter M, Korkmaz A, Oter S. Quercetin, a flavonoid antioxidant, prevents and protects streptozotocin-induced oxidative stress and β-cell damage in rat pancreas. Pharmacol Res 2005;51:117–23.
[43] Keane KN, Cruzat VF, Carlessi R, Debittencourt PI, Newsholme P. Molecular events linking oxidative stress and inflammation to insulin resistance and β-cell dysfunction. Oxid Med Cell Longev 2015;2015.
[44] Varasteh AR, Haghir H. Evaluation of bcl-2 family gene expression and caspase-3 activity in hippocampus stz-induced diabetic rats. Exp Diabetes Res 2008;12:2008.
[45] Al-Nahdi AM, John A, Raza H. Cytoprotective effects of N-acetylcysteine on streptozotocin-induced oxidative stress and apoptosis in RIN-5F pancreatic β-cells. Cell Physiol Biochem 2018;51:201–16.
[46] Kimani CN, Reuter H, Kotzé SH, Venter P, Ramharack P, Muller CJ. Pancreatic beta cell regenerative potential of Zanthoxylum chalybeum Engl. Aqueous stem bark extract. J Ethnopharmacol 2023:117374. Nov 7.
[47] Subash-Babu P, Ignacimuthu S, Alshatwi AA. Nymphayol increases glucose-stimulated insulin secretion by RIN-5F cells and GLUT4-mediated insulin sensitization in type 2 diabetic rat liver. Chem Biol Interact 2015;226:72–81.